Journal of Photochemistry and Photobiology A: Chemistry 224 (2011) 123–134

Contents lists available at SciVerse ScienceDirect

Journal of Photochemistry and Photobiology A: Chemistry

journal homepage: www.elsevier.com/locate/jphotochem

Spectroscopic characterization and photoinduced processes of 4-oxoquinoline derivatives

Zuzana Barbieriková[a], Maroš Bella[b], Jozef Lietava[a], Dana Dvoranová[a], Andrej Staško[a], Tibor Füzik[c,d], Viktor Milata[b], Soňa Jantová[c], Vlasta Brezová[a,*]

[a] Institute of Physical Chemistry and Chemical Physics, Faculty of Chemical and Food Technology, Slovak University of Technology, Radlinského 9, SK-812 37 Bratislava, Slovak Republic
[b] Institute of Organic Chemistry, Catalysis and Petrochemistry, Faculty of Chemical and Food Technology, Slovak University of Technology, Radlinského 9, SK-812 37 Bratislava, Slovak Republic
[c] Institute of Biochemistry, Nutrition and Health Protection, Faculty of Chemical and Food Technology, Slovak University of Technology, Radlinského 9, SK-812 37 Bratislava, Slovak Republic
[d] Department of Biochemistry and Microbiology, Faculty of Food and Biochemical Technology, Institute of Chemical Technology, Technická 5, CZ-166 28 Praha 6, Czech Republic

ARTICLE INFO

Article history:
Received 12 May 2011
Received in revised form
13 September 2011
Accepted 17 September 2011
Available online 29 September 2011

Keywords:
4-Oxoquinolines (quinolones)
UV/vis spectroscopy
FT-IR
Cathodic reduction
EPR spectroscopy
Spin trapping technique
Reactive oxygen species
Cytotoxic activity
HL-60 cells

ABSTRACT

Derivatives of 1,4-dihydro-4-oxoquinoline substituted at 4-pyridone or/and benzene moieties were synthesized (**Q1**–**Q17**), and characterized by UV/vis and FT-IR spectroscopy. In dimethylsulfoxide and acetonitrile solvents a significant influence of the substituent's character and position on the quinolone skeleton was observed on the absorption bands in the UVA region (315–400 nm). Electron-withdrawing substituents (nitro, cyano, acetyl or trifluoroacetyl) caused a red shift, resulting in the effective absorption of UVA light. Photoinduced generation of superoxide radical anion and singlet oxygen upon UVA irradiation was followed by EPR spectroscopy using *in situ* spin trapping technique; 4-hydroxy-2,2,6,6-piperidine (TMP) served for singlet oxygen ($^1O_2$) detection. An efficient generation of superoxide radical anions and singlet oxygen was observed predominantly for nitro-substituted quinolones. The effect of quinolones on proliferation of HL-60 cells was monitored, and the values of IC_{50} evidenced the highest inhibition in the presence of ethyl 1,4-dihydro-6-fluoro-8-nitro-4-oxoquinoline-3-carboxylate (**Q17**) and ethyl 1,4-dihydro-8-nitro-4-oxoquinoline-3-carboxylate (**Q5**).

1. Introduction

1,4-Dihydro-4-oxoquinoline derivatives (4-quinolones) represent one of the largest classes of antimicrobial agents, and many of them are used worldwide in medical care (e.g., ciprofloxacin, ofloxacin, levofloxacin, moxifloxacin, etc.) [1–6]. As far as the position and the number of substituents are considered, we can find diverse applications of commonly available quinolone drugs [7–10]. Specific members of this drug family also display high activity against eukaryotic type II topoisomerases, as well as against cultured mammalian cells [11,12]. These antineoplastic quinolones represent a prospective source of new anticancer agents [13–15]. Quinolone derivatives possessing a fluorine atom as a substituent have been classified as most efficient in biological activity [1,16–18]. Quinolone-type drugs are considered to be very well tolerated, revealing only limited adverse effects during therapy [16]. However, quinolones undergo degradation processes upon UV irradiation, leading to the loss of their antimicrobial activity [19–24]. Within these photochemical processes reactive oxygen species (ROS) are generated and these reactions may result in the emergence of side effects during antimicrobial therapy [25–27]. Since it has been established that quinolones reveal phototoxic activity, many commercially used antibiotics have been studied in order to classify their behavior upon UVA exposure [19,28–30]. In some cases photoinduced superoxide radical anion and singlet oxygen generation has been confirmed (e.g., lomefloxacin, enoxacin, ofloxacin and ciprofloxacin) [31–34]. In spite of all the negative

Abbreviations: ACN, acetonitrile; ATCC, American type culture collection; c_{rel}, relative concentration; DFT, density functional theory; DIPPMPO, 5-(diisopropoxy-phosphoryl)-5-methyl-1-pyrroline *N*-oxide; DBNBS, 3,5-dibromo-4-nitrosobenzenesulfonate, sodium salt; DMPO, 5,5-dimethyl-1-pyrroline *N*-oxide; DMSO, dimethylsulfoxide; EMPO, 5-ethoxycarbonyl-5-methyl-1-pyrroline *N*-oxide; EPR, electron paramagnetic resonance; FT-IR, Fourier Transform Infrared Spectroscopy; hfcc, hyperfine coupling constants; ROS, reactive oxygen species; SW, magnetic field sweep width; $TBAPF_6$, tetrabutylammonium hexafluorophosphate; TEA, triethylamine; Tempol, 4-hydroxy-2,2,6,6-tetramethylpiperidine *N*-oxyl; TMP, 4-hydroxy-2,2,6,6-tetramethylpiperidine; UV/vis, ultraviolet/visible.

* Corresponding author. Tel.: +421 2 5932 56 66; fax: +421 2 5932 57 51.
E-mail address: vlasta.brezova@stuba.sk (V. Brezová).

1010-6030/$ – see front matter © 2011 Elsevier B.V. All rights reserved.
doi:10.1016/j.jphotochem.2011.09.015

Table 1
Overview of the investigated quinolones with substitution specification.

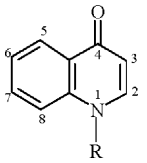

	Substitution character and position			
	N-1	C-3	C-6	C-8
Q1	H	H	H	H
Q2	H	$COOC_2H_5$	H	H
Q3	CH_3	$COOC_2H_5$	H	H
Q4	H	$COOC_2H_5$	NO_2	H
Q5	H	$COOC_2H_5$	H	NO_2
Q6	H	$COOC_2H_5$	$NHCOCH_3$	H
Q7	H	$COOCH_3$	H	H
Q8	CH_3	$COOCH_3$	H	H
Q9	C_2H_5	$COOCH_3$	H	H
Q10	H	COOH	H	H
Q11	CH_3	COOH	H	H
Q12	C_2H_5	COOH	H	H
Q13	H	CN	H	H
Q14	H	$COCH_3$	H	H
Q15	H	NO_2	H	H
Q16	H	$COCF_3$	H	H
Q17	H	$COOC_2H_5$	F	NO_2

effects of photoinduced ROS formation on the organism in the presence of these drugs, positive applications of this behavior have also been discovered, and new types of quinolones are applied in target therapeutic applications, as photosensitizers [21,28,35]. In this case ROS generation represents a powerful tool for selective cancer cell destruction [36–38]. Despite wide interest and research in this field, the mechanism of quinolone phototoxicity remains unexplained. As long as we assume that the phototoxic responses to photosensitized reactions of quinolones originate from ROS formation, it appears necessary to clarify how many and what types of these reactive species are formed. The phototoxicity of quinolones is obviously initiated by different mechanisms running through various pathways, dependent on different factors. Hence a great effort has been made to investigate the structure–phototoxicity relationship [21,22,30,39–41].

Presented paper summarizes spectral characteristics of synthesized 1,4-dihydro-4-oxoquinoline derivatives (**Q1**–**Q17**, Table 1) obtained by UV/vis and FT-IR spectroscopy. Their capability to generate reactive radical intermediates or singlet oxygen upon UVA irradiation was investigated by means of EPR spectroscopy. The cytotoxic effect of quinolones on the proliferation of HL-60 cells was monitored and the IC_{50} values for individual quinolones were determined.

2. Experimental

2.1. Materials

The substituted 1,4-dihydro-4-oxoquinoline derivatives were synthesized and purified in our laboratory as described in Ref. [42]. An overview of their structure and substituent characterizations, along with abbreviations for the quinolones investigated (**Q1**–**Q17**), are summarized in Table 1.

The spin trapping agent, 5,5-dimethyl-1-pyrroline *N*-oxide (DMPO) was purchased from Aldrich and distilled before application. 5-(Diisopropoxy-phosphoryl)-5-methyl-1-pyrroline *N*-oxide (DIPPMPO) and 5-ethoxycarbonyl-5-methyl-1-pyrroline *N*-oxide (EMPO) delivered by Alexis® Biochemicals were used without purification. All spin trapping agents were stored at −18 °C. 4-Hydroxy-2,2,6,6-tetramethylpiperidine (TMP) from Merck-Schuchardt was used as supplied. The concentration of photogenerated paramagnetic species was determined using solutions of 4-hydroxy-2,2,6,6-tetramethylpiperidine *N*-oxyl (Tempol; Aldrich) as calibration standards. Solutions were prepared in aprotic solvents, either dimethylsulfoxide (DMSO; SeccoSolv®, Merck) or acetonitrile (ACN; SeccoSolv® Merck), or in mixed solvent DMSO:methanol (SeccoSolv®, Merck). Sodium azide (analytical grade, Sigma–Aldrich) served as a singlet oxygen quencher.

2.2. Cell lines

The human leukemia HL-60 cells obtained from American type culture collection (ATCC; Rockville, MD, USA), grown in suspension at 37 °C in a humidified 5%-CO_2 and 95%-air atmosphere were supplemented with 10% (v/v) fetal calf serum, penicillin G (100 μmol L^{-1}) and streptomycin (100 μmol L^{-1}) in complete RPMI 1640 medium. The cells were plated on Petri dishes (diameter 60 mm) at a density of 3×10^5 cells per mL of the medium and incubated for 24 h prior to the experiments. All culture medium compounds were obtained from Sigma–Aldrich; bovine serum and fetal calf serum were obtained from the BIOCOM Company (Slovakia). The quinolone stock solutions for the incubation of the cells were prepared in DMSO and subsequently diluted in the cell culture medium. The final DMSO concentration in the medium was 0.1% (v/v; in both control and treated samples), so as not to affect cell viability.

2.3. Methods

2.3.1. UV/vis spectroscopy

The UV/visible spectra of the quinolones investigated in DMSO and ACN were recorded using a UV-3600 UV/vis spectrometer (Shimadzu, Japan) with a 1 cm square quartz cell. The electronic spectra of the quinolones in ACN in the presence of TMP (with composition identical to that in the EPR experiments) were measured using a 0.2 cm quartz cell.

2.3.2. FT-IR spectroscopy

Infrared spectra of the quinolones **Q1**–**Q17** in the region 4000–700 cm^{-1} were recorded with a Nicolet model NEXUS 470 FT-IR spectrometer at room temperature applying dry film method from ACN solutions using reflectance technique on horizontal crystal plate (HATR) or using KBr technique, where the crystalline sample was thoroughly mixed with KBr (for IR spectroscopy, Fluka) and so prepared mixture was pressed into a pellet. Simulations of selected spectra were performed by Thermo Scientific Peak Resolve software (included in Omnic 7.4 Thermo Fisher Scientific Inc.), which fits a number of individual synthetic peaks to a complex set of overlapping peaks in a spectrum.

2.3.3. Electrochemical in situ EPR experiments

The electrochemical EPR experiments were performed in 0.001 M solutions of quinolones in DMSO or in mixed solvent DMSO:methanol (1:1; v/v). To increase the conductivity of solutions, tetrabutylammonium hexafluorophosphate ($TBAPF_6$; Fluka) was added to obtain a 0.1 M salt concentration. The solutions thus prepared were carefully purged with argon and filled in a Varian electrolytic cell equipped with a platinum net and inserted in the cavity of a Bruker EMX EPR spectrometer working in the X-band. The electrolytic cell was polarized at −2.5 V directly in the EPR cavity TM-110 (ER 4103 TM) and the EPR spectra were measured *in situ*. Typical EPR spectrometer settings were: microwave frequency, 9.79 GHz; microwave power, 10.0 mW; center field, 347.7 mT; sweep width, 6–10 mT; gain, 5×10^5–1×10^6; modulation amplitude, 0.01–0.1 mT; scan, 42–168 s; time constant, 81.92 ms; number of scans, 1–10. The *g*-values in the range of

2.0048 were determined by simultaneous measurement of a reference standard containing Tempol.

2.3.4. Photochemical in situ EPR experiments

The formation of paramagnetic intermediates upon UVA irradiation of quinolones in DMSO was monitored by an EPR spin trapping technique as described previously in Refs. [43,44]. The photoinduced production of singlet oxygen during the excitation of quinolones was followed in ACN solutions in the presence of TMP [44]. The solutions of quinolones containing spin trapping agents or TMP were mixed directly before the EPR measurements, then carefully saturated with air using a slight air stream and immediately transferred to a small quartz flat cell (WG 808-Q, Wilmad-LabGlass, USA; optical cell length 0.04 cm) optimized for the TE_{102} cavity of the EPR spectrometer EMX (Bruker, Germany). The samples were irradiated at 295 K directly in the EPR resonator, and the EPR spectra were recorded *in situ* during continuous photoexcitation. The irradiation source was an HPA 400/30S lamp (400 W, Philips) [43]. Wavelengths below 300 nm were eliminated using a Pyrex filter (with a thickness of 1 mm). The UVA irradiance of the UV lamp, 6 mW cm^{-2}, within the EPR cavity was determined with a UVX radiometer (UVP, USA). The light flux emitted by the HPA lamp at 365 nm (3.1×10^{-8} mol s^{-1}) was also determined by ferrioxalate actinometry [45], using the appropriate glass filters (Schott Glaswerke, Germany). The concentration of photogenerated paramagnetic species was evaluated from the double-integrated EPR spectra based on the calibration curve obtained from the EPR spectra of the Tempol solutions. Typical EPR spectrometer settings in a standard photochemical experiment were: microwave frequency, 9.44 GHz; microwave power, 10.03 mW; center field, 335.0 mT; sweep width, 10–20 mT; gain, 4×10^4–1×10^6; modulation amplitude, 0.05–0.1 mT; scan, 20.97 or 41.94 s; time delay, 1.03 or 3.06 s; time constant, 5.12 or 20.48 ms. The *g*-values were determined within an uncertainty of ±0.0001 by the simultaneous measurement of a reference sample containing DPPH.

2.3.5. EPR spectra processing and simulation

The EPR spectra obtained were processed, analyzed and simulated using the Bruker software WinEPR and SimFonia and the Winsim2002 software freely available from the website of the National Institute of Environmental Health Sciences (NIEHS) (http://epr.niehs.nih.gov/) [46].

2.3.6. Antiproliferative impact of quinolones on HL-60 cells

HL-60 cells were inoculated onto Petri dishes (diameter 60 mm; 1.5×10^6 cells/dish) in the exponential phase of growth. After 24 h of incubation at 37 °C, the quinolone derivatives at various concentrations were added to the cells. Control cells were treated with DMSO, the final concentration of DMSO never exceeded 0.1% (v/v). Negative control (NC) experiments were performed using DMSO-free cell systems. Then the cells were cultured for 24, 48 and 72 h in an incubator in the dark. Cell viability was determined by 0.4% Trypan blue staining. Finally, the cell proliferation was determined by direct counting of cell numbers in a counting chamber. The relative inhibition of cell proliferation or degeneration of the cell population was calculated as described in Ref. [43]. The IC_{50} values (the quinolone concentration resulting in 50% of the cell proliferation that was recorded in the control experiments) were determined separately for each experiment using nonlinear regression (Origin 7.0, Microcal). The presented values were calculated from at least three independent experiments.

Table 2
UV/vis absorption maxima and their molar absorption coefficients of the investigated quinolones in dimethylsulfoxide and acetonitrile.

Quinolone	Dimethylsulfoxide		Acetonitrile	
	λ_{max} (nm)	$\varepsilon_{\lambda_{max}}$ (dm^3 mol^{-1} cm^{-1})	λ_{max} (nm)	$\varepsilon_{\lambda_{max}}$ (dm^3 mol^{-1} cm^{-1})
Q1	290	3 800	208	46 200
	318	9 700	238	22 300
	333	10 900	274	4 600
			285	5 900
			315	14 300
			328	16 100
Q2	311	13 900	211	27 400
			236	12 700
			247	12 700
			254	10 400
			308	10 900
Q3	316	12 400	213	27 900
			250	11 000
			257	10 400
			314	12 600
			327	10 600
Q4	387	22 600	235	10 600
			377	34 000
Q5	264	12 700	264	15 000
	387	6 500	384	8 000
Q6	333	20 800	225	12 300
			328	15 400
Q7	310	13 900	211	28 800
			247	10 800
			254	8 800
			308	9 800
Q8	315	13 900	212	38 200
			250	12 400
			256	11 600
			313	13 500
			327	11 200
Q9	316	10 600	213	33 000
			250	12 900
			256	11 900
			314	13 900
Q10	310	12 200	212	28 400
			247	18 300
			308	11 900
			320	9 300
Q11	315	13 600	213	19 100
	329	10 500	250	12 000
			256	11 500
			313	9 100
			327	7 500
Q12	315	8 100	214	24 800
	329	6 300	250	14 900
			256	14 100
			314	11 400
			327	9 400
Q13	276	12 200	221	6 800
	336	16 200	274	11 500
			331	14 600
Q14	320	8 500	251	4 900
			259	4 700
			312	6 300
Q15	313	9 600	215	18 200
	358	7 200	244	9 400
			311	8 100
			347	6 200
Q16	314	9 800	211	17 200
	328	8 400	243	12 800
			311	9 100
			325	8 100
Q17	268	21 100	212	22 300
	398	10 400	265	11 200
			395	5 500

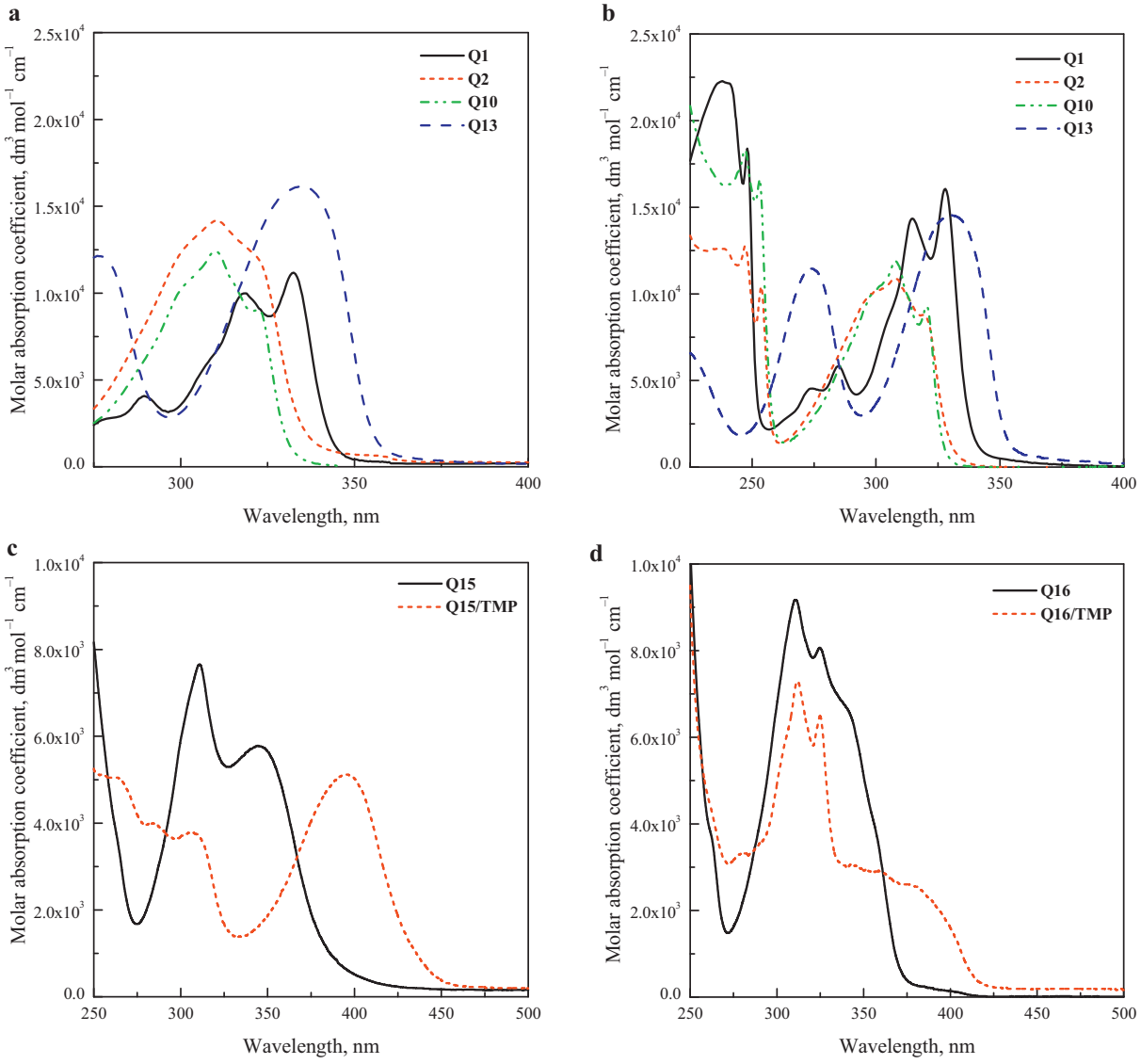

Fig. 1. Electronic absorption spectra of 1,4-dihydro-4-oxoquinoline (**Q1**) and its 3-substituted derivatives (**Q2**, **Q10**, **Q13**) in (a) DMSO, (b) ACN solutions. Changes of the UV/vis absorption spectra of (c) **Q15** and (d) **Q16** in the presence of TMP (c_{TMP} = 0.01 M) (ACN; optical path length 0.2 cm). (For interpretation of the references to color in this figure legend, the reader is referred to the web version of the article.)

3. Results and discussion

3.1. UV/vis absorption spectra of quinolones

The UV/vis absorption spectra of synthesized quinolones **Q1**–**Q17** (Table 1) measured in aprotic DMSO and ACN solvents, and the absorption maxima obtained with values of molar absorption coefficients are summarized in Table 2.

3.1.1. Dimethylsulfoxide

The electronic spectrum of the parent 4-oxoquinoline **Q1** in DMSO shows absorption maxima at wavelengths of 290, 318 and 333 nm, typical for $\pi \rightarrow \pi^*$ and $n \rightarrow \pi^*$ transitions [47]. The derivatives **Q2** and **Q3**, substituted at the 3-position ($COOC_2H_5$) and the 1-position (CH_3), show comparable UV/vis absorption with maxima at 311 and 316 nm, respectively. Derivatives **Q7**–**Q12**, with hydrogen, methyl or ethyl at the 1-position, and COOH or $COOCH_3$ at the 3-position (Table 1) reveal in DMSO solutions very similar electronic spectra, with absorption maxima in the range of 310–316 nm, with a shoulder at about 329 nm (Table 2). The presence of the electron-withdrawing nitro group on benzene (**Q4**, **Q5**, **Q17**) or 4-pyridone (**Q15**) moieties of quinolone skeleton results in significant red shift of the low-energy absorption bands to the wavelength range of 358–398 nm (Table 2). The absorption spectrum of **Q6** with $COOC_2H_5$ and $NHCOCH_3$ groups at the 3- and the 6-positions, is characterized with an intensive absorption maximum at 333 nm (Table 2). The analysis of the low-energy absorption maxima wavelengths showed that substitution at the 3-position (derivatives **Q2**, **Q10**, **Q13**–**Q16**) results in a marked red-shift for the electron withdrawing groups, e.g., NO_2 or $COCF_3$ (Table 2). The impact of the substituent's character on the electronic absorption spectra in DMSO solvent ($\lambda > 275$ nm) for quinolones substituted at the 3-position (**Q1**, **Q2**, **Q10** and **Q13**) is shown in Fig. 1a. The analysis of low-energy absorption maxima ($\lambda_{l-e,max}$) of quinolones substituted at the 3-position (**Q2**, **Q7**, **Q10**, **Q13**–**Q16**) shows a linear increase in $\lambda_{l-e,max}$ with increasing values of the Hammett parameter σ_p^+ [48,49].

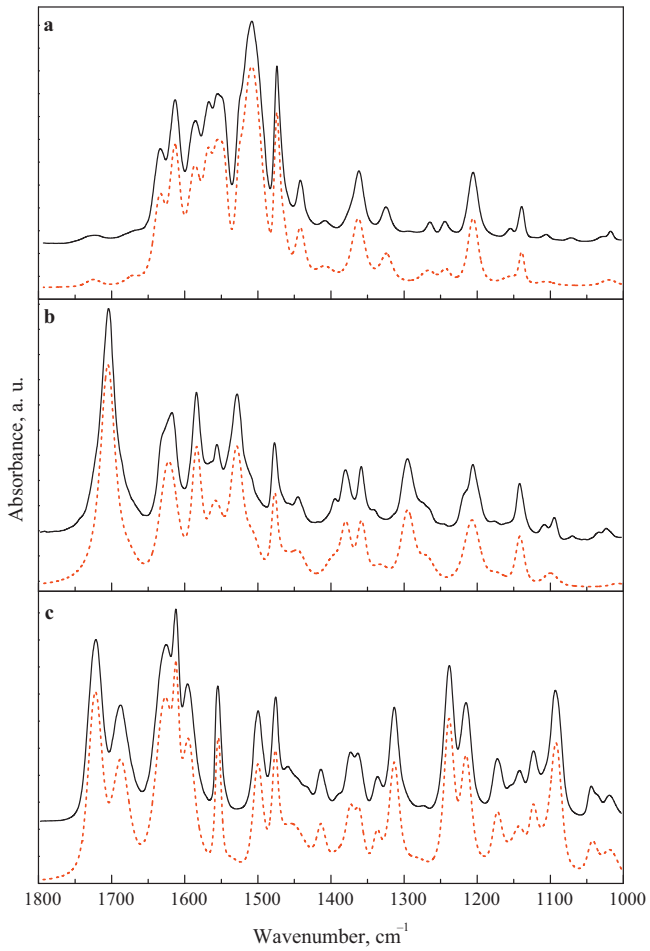

Fig. 2. Experimental (solid line) and simulated (dotted line) FT-IR spectra of quinolones: (a) **Q1**, (b) **Q2** and (c) **Q3** measured using dry film method in the region 1800–1000 cm^{-1}.

3.1.2. Acetonitrile

The UV/vis absorption spectrum of the unsubstituted quinolone **Q1** in ACN exhibits maxima at wavelengths 328, 315, 285, 274 and 238 nm [50]. The derivative **Q2** ($COOC_2H_5$ at the 3-position) demonstrates a blue shift with absorption bands at 308, 254, 247 and 236 nm. Further replacement of hydrogen at the 1-position with a methyl group (**Q3**) causes, in comparison with **Q2**, a smaller red shift, as absorption maxima were observed at 327, 314, 257 and 250 nm. Derivatives **Q7**–**Q12**, reveal very similar electronic spectra with absorption maxima in the spectral region 320–328, 308–316, 254–256 and 247–250 nm (Table 2). Significant bathochromic effects were evidenced in the presence of a nitro group at the 6-position (**Q4**; λ_{max} = 377 nm), at the 8-position (**Q5**; λ_{max} = 384 nm), at the 3-position (**Q15**; λ_{max} = 347 nm), as well as for derivative **Q17** ($COOC_2H_5$ at the 3-position, F at the 6-position and NO_2 at the 8-position; λ_{max} = 395 nm). The UV/vis spectrum of **Q6** ($COOC_2H_5$ at the 3-position and $NHCOCH_3$ at the 6-position) is characterized by an intensive absorption band with a maximum at 328 nm (Table 2). The effect of substitution at the 3-position on the electronic spectra measured in acetonitrile ($\lambda > 225$ nm) for derivatives **Q1**, **Q2**, **Q10** and **Q13** is illustrated in Fig. 1b. The presence of the cyano group at the 3-position (**Q13**) induces absorption at 331 nm, and additional peaks are found at 274 and 221 (Fig. 1b). Substitution at the 3-position with an electron-withdrawing nitro group (**Q15**) results in a red shift with a low-energy maximum at 347 nm (Fig. 1c). Analogously, the presence of $COCF_3$ at the 3-position (**Q16**), gives rise to a broad absorption band at 311 nm, along with indistinct maxima at 325 and 342 nm (Fig. 1d). Also in acetonitrile, a linear relationship between $\lambda_{l-e,max}$ and the Hammett parameter σ_p^+ was found for a quinolone series substituted at the 3-position (**Q2**, **Q7**, **Q10**, **Q13**–**Q16**).

The evaluation of the quantum yield/efficiency [51,52] of photochemical processes requires a precise determination of light flux absorbed by the photoexcited reagent under given experimental conditions [45]. The photoinduced generation of singlet oxygen upon UVA excitation was monitored here in acetonitrile *via* EPR spectroscopy, using a cyclic amine TMP as a singlet oxygen quencher [53]. The addition of TMP can cause absorption changes due to its interaction with quinolone molecules; consequently, we measured all UV/vis spectra of quinolones in acetonitrile solutions, which accurately reflect the composition of the solutions applied to EPR experiments. Changes in the electronic spectra of quinolones upon the addition of TMP were observed for derivatives **Q5**, **Q10**, **Q15**–**Q17**; no alterations in the spectral region 250–500 nm were found for other derivatives. The spectral changes of carboxylic acid **Q10** are coupled with an absorbance decrease at 308 and 320 nm, with simultaneous growth at 337 nm with isosbestic points at 279 and 322 nm (data not shown). It should be noted here, that for carboxylic acids **Q11** and **Q12** with a methyl or ethyl group at the 1-position, no changes in the presence of TMP were observed. Most probably, the presence of a hydrogen atom at the 1-position plays an important role in these reactions. Derivatives **Q5** and **Q17**, containing a nitro group at the 8-position, i.e., in the vicinity of the hydrogen at the N-1 position, reveal in the presence of TMP a similar decrease of the absorption band at 387 or 398 nm, coupled with an absorbance increase at 340 nm (data not shown), but no new absorption bands were formed. The investigated quinolones exhibit in solution two possible tautomers, representing hydroxy/oxo tautomers, as a result of a potential hydrogen transfer from N-1 nitrogen atom to oxo-group at carbon C-4 [44,54]. We assume that the addition of TMP can cause the changes in the tautomer's concentrations for **Q5** and **Q17** [47], as the presence of nitro group is responsible for the stabilization of the oxo-tautomeric form *via* the intramolecular interaction [55]. Recently, we performed the theoretical (DFT) and spectroscopic (UV/vis and FT-IR) investigations of the tautomeric forms of ethyl 1,4-dihydro-4-oxoquinoline-3-carboxylate (**Q2**) and its 8-nitro derivatives (**Q5** and **Q17**) [55]. The experimental electronic spectra of quinolones measured in aprotic solvents with various dielectric constants (toluene, 2.38; acetonitrile, 37.5; dimethylsulfoxide, 46.7) were interpreted using DFT including the solvent effects. The results of calculation confirmed the dominance of **Q2**, **Q5** and **Q17** oxo-tautomers in polar solvents, but in non-polar toluene the existence of hydroxy-tautomer is preferred for **Q2** [55].

On the other hand, quinolones **Q15** and **Q16**, at the 3-position, containing strongly electron withdrawing groups, i.e., NO_2 or $COCF_3$, interact with TMP in acetonitrile solution most probably *via* a charge transfer (CT) mechanism [50], producing new low-energy CT absorption bands at 400 nm for **Q15** (Fig. 1c), and at 382 nm for **Q16** (Fig. 1d), respectively.

3.2. FT-IR spectra of quinolones

Table 3 summarizes the selected vibration characteristics found in the FT-IR spectra of quinolone derivatives **Q1**–**Q17** considering the dominant existence of oxo-tautomers of NH-derivatives in the solid state [54]. Due to the large number of vibration modes, detailed mapping of the FT-IR spectra is complex, and consequently, only some of the main frequencies were attributed to the characteristic vibrations. Comparing the main frequencies, the stretching vibration of N–H can be found in region 3275–3160 cm^{-1}. The stretching vibration of ester group C=O is between 1725 and 1710 cm^{-1} (**Q2**–**Q9**, **Q17**)

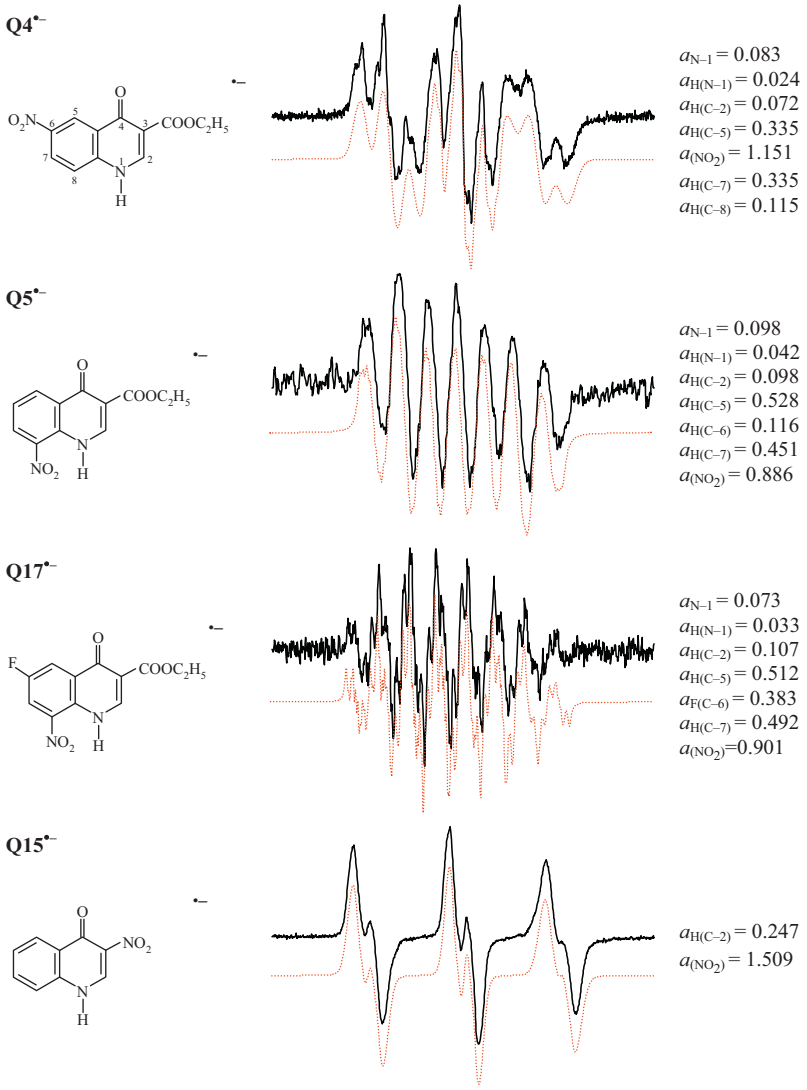

Fig. 3. Experimental (solid line) and simulated (dotted line) EPR spectra (*SW* = 6 mT) of nitro-substituted quinolones obtained upon the cathodic reduction of 0.001 M solutions of quinolones in DMSO (**Q4**, **Q15**) or methanol/DMSO (1:1; v/v) (**Q5**, **Q17**) along with the assignment of hyperfine coupling constants (in mT).

and stretching vibration of carboxylic acid group C=O is at 1730–1720 cm^{-1} (**Q10**–**Q12**). The stretching vibration of C=O group on pyridone ring of pristine quinolone **Q1** is 1637 cm^{-1}, but the substitution on the pyridone or/and benzene moieties causes the shift of this vibration to the lower values in the range 1625–1600 cm^{-1}. The stretching vibrations of conjugated C=C are situated in the region between 1650 and 1400 cm^{-1} [54–60]. For illustrations, Fig. 2 shows the experimental and simulated

Table 3
Selected vibrations of investigated quinolones **Q1**–**Q17** obtained from FT-IR spectra.

	Vibration wavenumber (cm^{-1})
Q1	3233 (NH), 3061, 1637 (C=O), 1621, 1593, 1547, 1507, 1474, 1440, 827, 758
Q2	3160 (NH), 3065, 1710 (C=O, ester), 1698, 1621, 1591, 1553, 1529, 1475, 1441, 1287, 804, 763
Q3	3035, 1720 (C=O, ester), 1688, 1625, 1612, 1569, 1584, 1555, 1500, 1475, 1459, 1414, 1238, 763
Q4	3233 (NH), 3081, 1725 (C=O, ester), 1685, 1632, 1606, 1595, 1510 (NO_2), 1502, 1484, 1469, 1441, 1414, 1315 (NO_2), 1272, 847, 750
Q5	3219 (NH), 3080, 1713 (C=O, ester), 1685, 1630, 1606, 1567, 1515 (NO_2), 1502, 1464, 1443, 1420, 1319 (NO_2), 1288, 777, 745
Q6	3323 (NH–C=O), 3273 (NH), 3088, 1716 (C=O, ester), 1702 (NH–C=O), 1689, 1672, 1659, 1632, 1617, 1589, 1544, 1517, 1488, 1440, 1411, 1280, 800, 478
Q7	3160 (NH), 3084, 1725 (C=O, ester), 1710, 1695, 1628, 1616, 1589, 1563, 1533, 1477, 1442, 1415, 1297, 805, 760
Q8	3054, 1724 (C=O, ester), 1677, 1632, 1624, 1610, 1595, 1553, 1503, 1475, 1457, 1442, 1414, 1243, 771, 756
Q9	3046, 1721 (C=O, ester), 1687, 1634, 1621, 1609, 1597, 1552, 1488, 1464, 1435, 1414, 1231, 763, 755
Q10	3265, 3223, 3175 (NH), 3098, 3031, 1720 (C=O, acid), 1695, 1634, 1618, 1581, 1548, 1518, 1494, 1476, 1446, 1414, 1237, 810, 767
Q11	3059, 1728 (C=O, acid), 1716, 1694, 1621, 1543, 1532, 1495, 1475, 1445, 1414, 1233, 808, 766
Q12	3098, 3052, 1725 (C=O, acid), 1710, 1690, 1615, 1551, 1514, 1494, 1469, 1427, 1414, 1226, 812, 763
Q13	3205 (NH), 3005, 2217 (C≡N), 1730, 1685, 1643, 1616, 1592, 1513, 1498, 1430, 1327, 1221, 789
Q14	3323 (NH), 3021, 1652 (C=O, oxo), 1641, 1621, 1589, 1567, 1540, 1514, 1478, 1448, 1403, 755
Q15	3197 (NH), 3063, 1645, 1628, 1614, 1597, 1539 (NO_2), 1493, 1474, 1448, 1341 (NO_2), 764
Q16	3164 (NH), 3075, 1708 (C=O), 1692, 1626, 1585, 1560, 1541, 1477, 1445, 1415, 469
Q17	3253 (NH), 3082, 1715 (C=O, ester), 1690, 1640, 1606, 1576, 1541, 1514 (NO_2), 1465, 1445, 1407, 1312 (NO_2), 744

FT-IR spectra of quinolones **Q1**, **Q2** and **Q3** obtained using dry film method.

3.3. Cathodic reduction of quinolones (in situ EPR experiments)

Cathodic reduction of quinolones **Q1**–**Q17** in the deoxygenated DMSO solutions was performed with the aim of generating corresponding radical anions, and to monitor *in situ* their EPR spectra. However, under the given experimental conditions, only radical anions of nitro substituted quinolones (**Q4**, **Q5**, **Q17** and **Q15**) were evident. Fig. 3 shows the obtained experimental EPR spectra along with their simulations and the spin Hamiltonian parameters used in the simulated spectra calculations. The EPR spectra of **Q4**$^{\bullet-}$, **Q5**$^{\bullet-}$ and **Q17**$^{\bullet-}$, with a nitro group at the 6- or the 8-position of the quinolone molecule, indicate the interaction of an unpaired electron (characterized with highest spin density at the NO_2 group) with N-1 nitrogen ($a_{N\text{-}1}$ = 0.073–0.098 mT), and with hydrogen nuclei at both, i.e., benzene and 4-pyridone moieties. In the EPR spectrum of **Q4**$^{\bullet-}$ (Fig. 3) hyperfine coupling constants (hfcc) of NO_2 ($a_{(NO_2)} = 1.151$ mT) dominate, along with the hfcc of two equivalent hydrogen nuclei in its *ortho* positions ($a_{H(C\text{-}5)} = a_{H(C\text{-}7)} = 0.335$ mT). Analogously, in the EPR spectrum of **Q5**$^{\bullet-}$ (Fig. 3), besides the hfcc of NO_2 ($a_{(NO_2)} = 0.886$ mT), the hydrogen nuclei in the *ortho* and *para* positions are also clearly detectable ($a_{H(C\text{-}7)} = 0.451$ mT; $a_{H(C\text{-}5)} = 0.528$ mT). The hyperfine coupling constants of further hydrogen nuclei are significantly lower, in agreement with reference data [61–63]. The EPR spectrum of **Q17**$^{\bullet-}$ (Fig. 3) is fully compatible with **Q5**$^{\bullet-}$, except that the hfcc of hydrogen at the 6-position ($a_{H(C\text{-}6)} = 0.116$ mT) is replaced by a value corresponding to one fluorine nucleus ($a_{F(C\text{-}6)} = 0.383$ mT). The EPR spectrum measured upon cathodic reduction of **Q15**, possessing a nitro group at the 3-position, is less complex (Fig. 3), reflecting only the interaction of an unpaired electron with the nitro group ($a_{(NO_2)} = 1.509$ mT) and one hydrogen nucleus in the *ortho* position ($a_{H(C\text{-}2)} = 0.247$ mT).

3.4. Photoinduced processes of quinolones investigated by EPR spin trapping technique

The generation of paramagnetic species upon UVA photoexcitation of quinolones was investigated in DMSO using spin trapping agents DMPO, DIPPMPO or EMPO.

Fig. 4a shows the EPR spectra monitored upon prolonged irradiation of DMSO solutions of **Q17** in the presence of DMPO. The dominating photoinduced twelve-line EPR signal is characterized by the spin Hamiltonian parameters a_N = 1.275 mT, $a_H{}^{\beta}$ = 1.033 mT, $a_H{}^{\gamma}$ = 0.139 mT and g = 2.0059 (Fig. 5a), which are in good agreement with the hyperfine coupling constants attributed to the •DMPO–$O_2{}^-$ spin adduct in DMSO [44,64–66]. Simulation analysis of the experimental spectra obtained revealed that, in addition to the major spin adduct •DMPO–$O_2{}^-$, the spin adduct •DMPO–OCH_3 (a_N = 1.314 mT, $a_H{}^{\beta}$ = 0.816 mT, $a_H{}^{\gamma}$ = 0.178 mT and g = 2.0059) is also generated simultaneously, and its concentration increased upon prolonged exposure, as documented in Fig. 5a after 10 min of irradiation. The generation of •DMPO–OCH_3 has been previously observed in systems containing DMSO and DMPO, where the radical species $O_2{}^{\bullet-}$/•OOH or hydrogen peroxide were generated [44,67].

The time-monitored EPR spectra measured upon photoexcitation of **Q4** in aerated DMSO solutions in the presence of DMPO are depicted in Fig. 4b. The UVA photoexcitation results in the generation of spin adducts •DMPO–$O_2{}^-$ and •DMPO–OCH_3 at the beginning of photoexcitation. But further species added to DMPO are also evident in the experimental EPR spectra, as documented in Fig. 5b, after 1 min and after 10 min of UVA irradiation of solution **Q4**/DMSO/DMPO/air. The experimental EPR spectrum obtained was analyzed, and described by simulation,

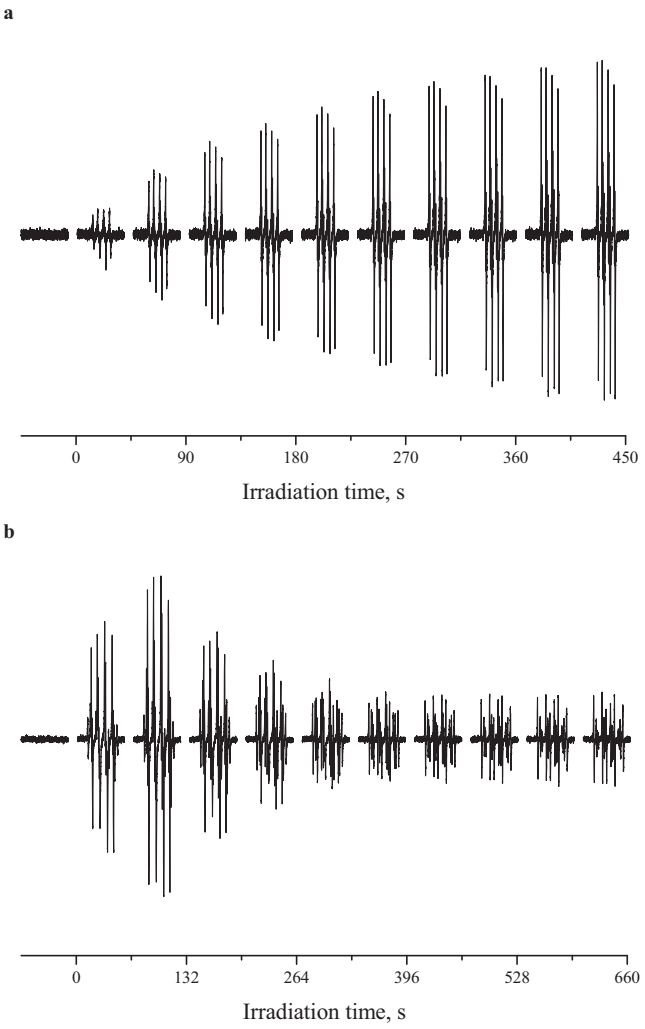

Fig. 4. The time-evolution of the EPR spectra (*SW* = 10 mT) monitored upon photoexcitation (λ > 300 nm) of aerated DMSO solutions of quinolones ($c_{0,\mathbf{Q}}$ = 3.2 mM) in the presence of spin trapping agent DMPO ($c_{0,DMPO}$ = 0.04 M): (a) **Q17** and (b) **Q4**.

representing a linear combination of five individual EPR signals attributed to •DMPO–$O_2{}^-$, •DMPO–OCH_3, •DMPO–OR, •DMPO–CR_1 and •DMPO–CR_2 (Fig. 5b). Most probably, UVA photoexcitation of **Q4** under the given experimental conditions initiates damage to the quinolone skeleton *via* ROS, coupled with the formation of further radical intermediates (oxygen- and carbon-centered radicals).

The photoinduced formation of •DMPO–$O_2{}^-$ and •DMPO–OCH_3 was also observed upon the irradiation of quinolone derivatives **Q4**–**Q6**, **Q13**–**Q17**, with structures enabling an adequate absorption of excitation radiation (λ_{max} = 365 nm). Otherwise, due to the low absorption of excitation radiation under the given experimental conditions, photoinduced generation of radical intermediates and their spin adducts was negligible upon irradiation of **Q1**–**Q3**, **Q7**–**Q12**.

In order to verify the assignment of spin adducts monitored using DMPO (Figs. 4 and 5), additional EPR experiments using DIPPMPO and EMPO spin trapping agents were performed. Unfortunately, their application is mainly oriented on aqueous systems [68], and the hfcc's published on spin adducts in other solvents are limited [69]. The chiral center in DIPPMPO and EMPO may result in the generation of *trans* and *cis* diastereoisomers of spin adducts characterized by different EPR spectra [70,71], causing difficulties in the simulation analysis.

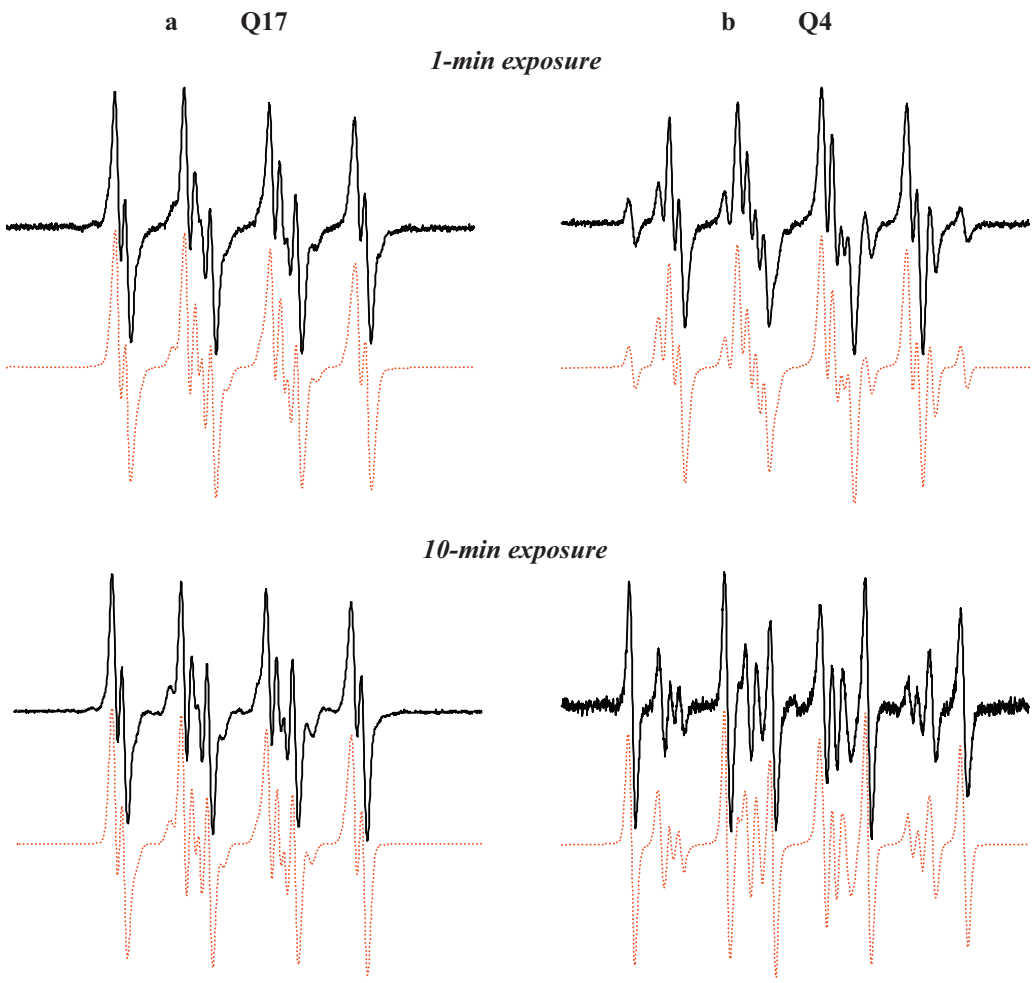

Fig. 5. Experimental (solid line) and simulated (dotted line) EPR spectra (*SW* = 7 mT) obtained after a 1-min or a 10-min photoexcitation of aerated 3.2 mM: (a) **Q17** and (b) **Q4** quinolones in DMSO solutions in the presence of DMPO ($c_{0,DMPO}$ = 0.04 M). Spin Hamiltonian parameters from simulations (hfcc in mT and relative concentrations in %) are: (a) **Q17**, *1-min*: •DMPO–$\mathbf{O_2}^-$ (a_N = 1.275, a_H^β = 1.033, a_H^γ = 0.139; *g* = 2.0059; 91%), •DMPO–$\mathbf{OCH_3}$ (a_N = 1.314, a_H^β = 0.816, a_H^γ = 0.178; *g* = 2.0059; 9%); *10-min*: •DMPO–$\mathbf{O_2}^-$ 81% and •DMPO–$\mathbf{OCH_3}$ 19%. (b) **Q4**, *1-min*: •DMPO–$\mathbf{O_2}^-$ 69%, •DMPO–$\mathbf{OCH_3}$ 14%, •DMPO–**OR** (a_N = 1.295, a_H^β = 1.417; *g* = 2.0059; 12%), •DMPO–$\mathbf{CR_1}$ (a_N = 1.433, a_H^β = 2.120; *g* = 2.0057; 5%); *10-min*:•DMPO–$\mathbf{O_2}^-$ 27%, •DMPO–$\mathbf{OCH_3}$ 2%, •DMPO–**OR** 21%, •DMPO–$\mathbf{CR_1}$ 34%, •DMPO–$\mathbf{CR_2}$ (a_N = 1.400, a_H^β = 2.113; *g* = 2.0057; 16%).

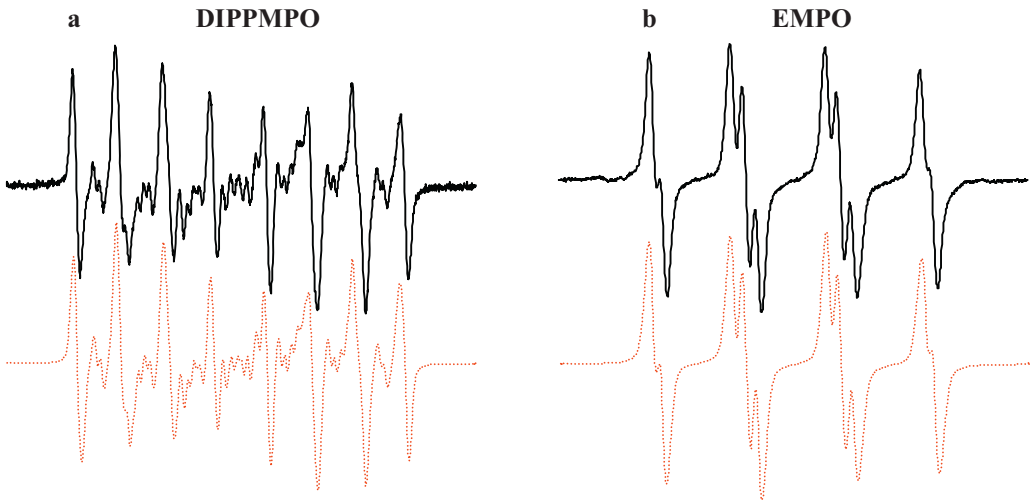

Fig. 6. Experimental (solid line) and simulated (dotted line) EPR spectra obtained after a 10-min photoexcitation of aerated DMSO solutions of **Q17** ($c_{0,\mathbf{Q17}}$ = 3.2 mM) in the presence spin trapping agents: (a) DIPPMPO ($c_{0,DIPPMPO}$ = 0.01 M) and (b) EMPO ($c_{0,EMPO}$ = 0.01 M). Spin Hamiltonian parameters from simulations (hfcc in mT and rel. concentration in %) are: (a) DIPPMPO (*SW* = 12 mT): *trans*-•DIPPMPO–$\mathbf{O_2}^-$ (a_P = 4.833, a_N = 1.219, a_H^β = 1.027, a_H^γ = 0.094; *g* = 2.0059; 35%), *cis*-•DIPPMPO–$\mathbf{O_2}^-$ (a_P = 4.917, a_N = 1.174, a_H^β =1.230, a_H^γ = 0.091; *g* = 2.0059; 10%), *trans*-•DIPPMPO–$\mathbf{OCH_3}$ (a_P = 4.677, a_N = 1.346, a_H^β = 1.101; *g* = 2.0059; 38%) and *cis*-•DIPPMPO–$\mathbf{OCH_3}$ (a_P = 3.760, a_N = 1.271, a_H^β = 0.959, a_H^γ = 0.147; *g* = 2.0059; 17%). (b) EMPO (*SW* = 6 mT): *trans*-•EMPO–$\mathbf{O_2}^-$ (a_N = 1.203, a_H^β =1.182; *g* = 2.0059; 64%) and *trans*-•EMPO–$\mathbf{OCH_3}$ (a_N = 1.218, a_H^β =0.902; *g* = 2.0059; 36%).

The experimental and simulated EPR spectra obtained after a 10-min exposure of aerated DMSO solution of **Q17** in the presence of DIPPMPO are shown in Fig. 6a. Simulation analysis evidenced, analogously to DMPO, the generation of $O_2^{\bullet -}$, and individual simulation spectra were attributed to *trans*- and *cis*-isomers of $^{\bullet}$DIPPMPO–O_2^- and $^{\bullet}$DIPPMPO–OCH_3.

The experimental and simulated EPR spectra obtained after a 10-min exposure in the irradiated DMSO solutions of **Q17** in the presence of EMPO is illustrated in Fig. 6b. The spectrum represents a linear combination of two individual paramagnetic species, attributed to *trans*-$^{\bullet}$EMPO–O_2^- (a_N = 1.203 mT, a_H^{β} = 1.182 mT; g = 2.0059) and *trans*-$^{\bullet}$EMPO–OCH_3 (a_N = 1.218 mT, a_H^{β} = 0.902 mT; g = 2.0059), assuming no hyperfine splittings of γ-hydrogens in accordance with Ref. [68].

3.5. Photoinduced singlet oxygen generation by quinolones

The photoinduced generation of singlet oxygen upon continuous irradiation of quinolones in aerated solutions was monitored *via* the oxidation of TMP to a semi-stable nitroxide radical Tempol characterized with a three-line EPR signal (a_N = 1.575 mT; g = 2.0060) [67,72]. Sufficient solubility of the investigated quinolones in DMSO, and the capability of this aprotic solvent to stabilize photogenerated superoxide radical anions, enabled us to perform spin trapping experiments and to detect the generation of paramagnetic intermediates, as described above. Subsequently, we irradiated quinolone DMSO/TMP/air systems in order to monitor and to quantify the photoinduced generation of Tempol, which reflects the $^1O_2$ production in the system. Fig. 7a shows the time-evolution of EPR spectra measured upon photoexcitation of **Q4**/DMSO/TMP/air solution. The Tempol was generated during the initial period of exposure, then reached a maximum, and decreased upon prolonged photoexcitation. This time-evolution can be explained by taking into account the simultaneous generation of superoxide radical anions and further oxygen- and carbon-centered paramagnetic species, which interact with Tempol and generate diamagnetic products, resulting in a decrease of the Tempol EPR signal [73,74].

Acetonitrile is, due to the higher solubility of molecular oxygen [75,76] and the satisfactory lifetime of singlet oxygen [77], an appropriate solvent to monitor the generation of $^1O_2$. The photoexcitation of the investigated quinolones was carried out in ACN/TMP/air solutions, and no decline of photogenerated Tempol upon prolonged irradiation under the given experimental conditions was observed. The increasing generation of Tempol EPR signal upon photoexcitation of **Q4** is shown in Fig. 7b, with significant EPR line-broadening compared to DMSO due to the higher solubility of molecular oxygen in acetonitrile [75,76].

The relative integral intensities of the EPR signal were obtained by double-integration of the individual experimental spectra, and the calculated concentration of photogenerated Tempol upon UVA exposure is shown in Fig. 8a for derivatives **Q1**–**Q7**. The dependencies of Tempol concentration upon irradiation time found were fitted by a non-linear least-squares method to Boltzmann function, and the initial rate of photoinduced Tempol formation ($R_{in,Tempol}$) was evaluated for all quinolones. The $R_{in,Tempol}$ values were used to compute quantum efficiency (300–400 nm) of Tempol formation *via* singlet oxygen oxidation of TMP [45]. The highest values of quantum efficiency (300–400 nm) of photoinduced Tempol generation (QE_{Tempol}) were found for **Q4** (4.1×10^{-4}), followed by **Q5** (1.0×10^{-4}) and **Q14** (6.4×10^{-5}). The QE_{Tempol} values for other derivatives varied in the range of 0–1.0×10^{-5}. The oxidation of TMP *via* $^1O_2$ upon irradiation of reaction system **Q17**/ACN/TMP/air was confirmed by the addition of NaN_3, acting as a $^1O_2$ quencher. The presence of NaN_3 resulted in a substantial decrease of the EPR signal intensity of photogenerated Tempol as shown in Fig. 8b.

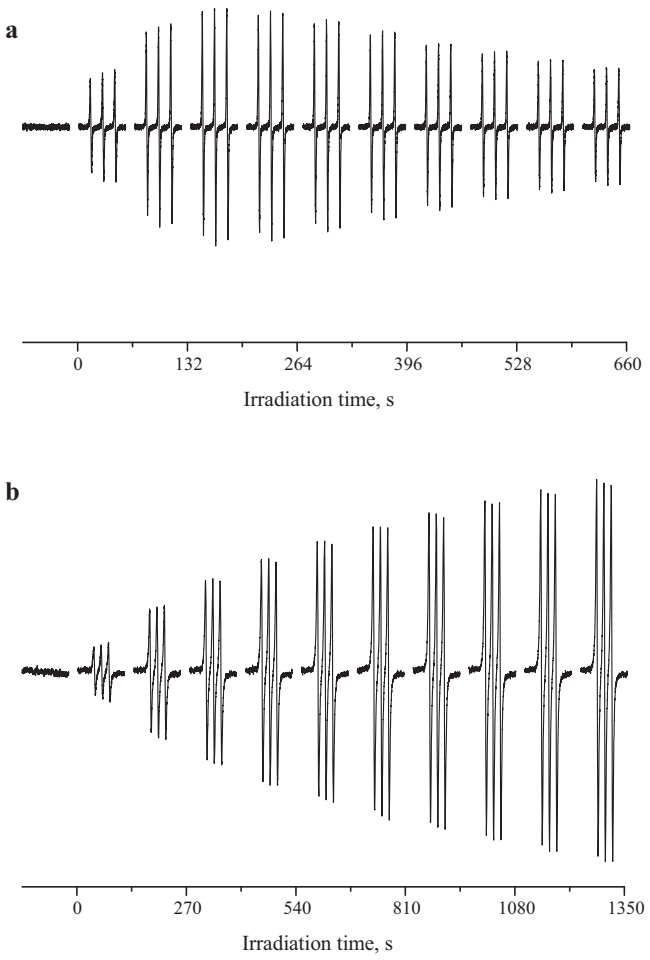

Fig. 7. The time-monitored EPR spectra (SW = 10 mT) upon progressing photoexcitation (λ > 300 nm) of **Q4** in the presence of 0.01 M TMP in aerated solutions: (a) DMSO; (b) ACN.

The EPR investigations showed that upon absorption of UVA radiation investigated 4-oxoquinolines behave as photosensitizers, and that the photoinduced activation of molecular oxygen generating superoxide radical anion and singlet oxygen represents important process in the aerated solutions. The photogenerated ROS interact with solvent or quinolone molecules producing unstable paramagnetic intermediates as was evidenced using EPR spin trapping technique, but other processes of quinolones in the excited states coupled with radical production cannot be excluded [30].

3.6. The antiproliferative effect of quinolones on HL-60 cells

The quinolone concentrations inducing 50% inhibition of the cell proliferation in comparison to the control (IC_{50}) was estimated and results are summarized in Table 4. The cells without presence of DMSO and quinolones were used as a negative control. *Cis*-diaminedichloroplatinum (II) (cisplatin) was used as a positive control. The obtained values show that the cytotoxic activity of all quinolones is lower than the positive control. On the other hand, significant cytotoxic/antiproliferative activity on human promyelocytic leukemia cell line HL-60 was found for quinolones **Q1**, **Q2**, **Q5**, **Q8**, **Q9**, **Q13**, **Q16** and **Q17**. The obtained values show that HL-60 cells were the most sensitive to the presence of 8-nitro derivatives **Q5** and **Q17**, in correlation with known pharmacophoric features of the nitro and fluoro groups.

In our preliminary study, we evidenced that the presence of quinolone **Q5** induced direct DNA strand breaks in leukemia L1210

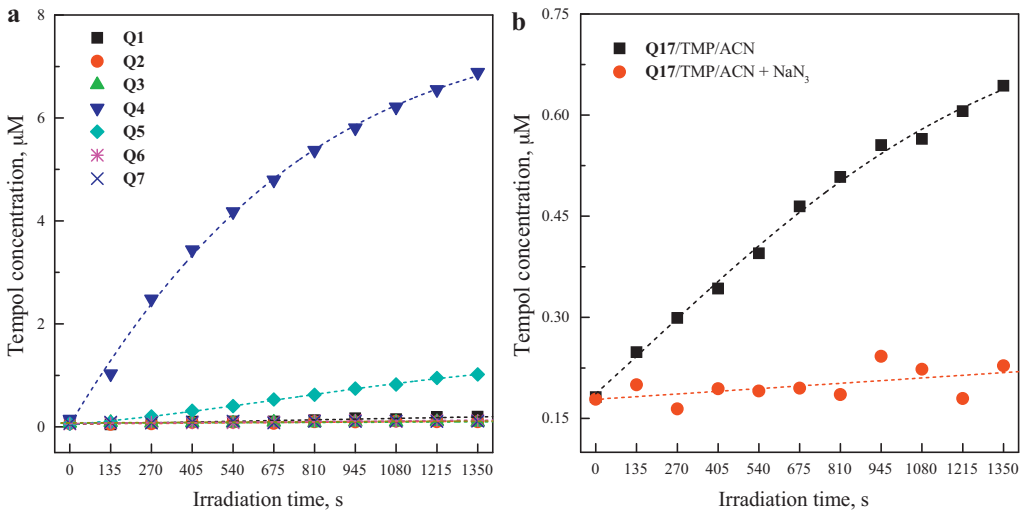

Fig. 8. (a) Concentration of nitroxide radical Tempol generated upon progressing irradiation *via* oxidation of TMP in aerated ACN solutions of quinolones **Q1**–**Q7** ($c_{0,TMP}$ = 0.01 M). The symbols represent the experimental data and dashed lines their mathematical simulations using least squares analysis. (b) Impact of sodium azide (●) addition on the concentration of Tempol radical generated upon progressing irradiation of **Q17** in aerated ACN solutions ($c_{0,TMP}$ = 0.01 M). (■) Solution **Q17**/ACN/TMP/air without NaN_3.

cells, and this effect was increased upon UVA irradiation [78]. The DNA damage generated by **Q5** caused the cell arrest in G_0/G_1 and G_2/M phases, decrease of cells number in S phase and apoptotic cell death of certain part of cell population after 24 h of influence. Quinolone **Q5** in combination with UVA irradiation induced apoptosis in leukemia cells through ROS-dependent mitochondrial pathway [78].

At present, biological experiments with non-photoactivated and UVA photoactivated quinolones **Q16** and **Q17** on leukemia cell lines are performed, focusing our attention on the role of ROS. As suggested by reviewer, also nitric oxide can be liberated during the photoexcitation of nitro-quinolones increasing their cytotoxicity, consequently further EPR measurements with the iron-dithiocarbamate complexes for NO detection [79] could be supplemented in future.

Table 4
Concentrations of investigated quinolones inducing 50% (IC_{50}) inhibition of the growth of HL-60 cells after 24, 48 or 72 h of cultivation.

Quinolone	IC_{50} (μmol L^{-1})		
	Time (h)		
	24	48	72
Q1	290	>690	>690
Q2	140	150	160
Q3	>430	>430	>430
Q5	31	48	58
Q6	120	>180	30
Q7	>245	>245	>245
Q8	260	>460	>460
Q9	170	>430	>430
Q10	>130	>130	>130
Q13	290	>590	>590
Q14	>530	>530	>530
Q15	>260	>260	>260
Q16	110	33	17
Q17	3.1	4.4	3.9
PC (cisplatin)[a]	2.6	2.5	2.1

[a] The cells growing in the presence of cisplatin were used as a positive control (PC), the cells without presence of DMSO and quinolones were used as a negative control.

4. Conclusions

4-Oxoquinolone derivatives containing different substituents at 4-pyridone and/or benzene moieties were synthesized as potential antimicrobial and anticancer agents. The UV/vis absorption spectra measured in dimethylsulfoxide and acetonitrile demonstrated that the peak positions and their intensities are mainly influenced by the substituent's character. The presence of nitro, cyano or acetyl groups at the 3-position caused a red shift of low-energy absorption maxima, and enabled efficient absorption of UVA radiation by quinolone molecules. EPR investigations evidenced that UVA photoexcited quinolones reveal the ability to photoactivate molecular oxygen *via* an electron/energy transfer mechanism generating superoxide radical anions and singlet oxygen. In the cathodically initiated electron transfer anion radicals from nitro-substituted derivatives were observed. Biological studies have shown that some quinolines demonstrated significant cytotoxic/antiproliferative activity on human promyelocytic leukemia HL-60 cells. The most effective were derivatives possessing a nitro group at the 8-position.

Acknowledgements

This study was financially supported by the Scientific Grant Agency (VEGA Projects 1/0660/11, 1/0018/09) and the Research and Development Agency of the Slovak Republic (contracts No. APVV-0055-07, APVV-0339-10 and SK-AT-0016-08). Zuzana Vrecková and Michal Lendel are gratefully acknowledged for technical assistance and Philip Grier for helpful discussion.

References

[1] M. Koba, T. Baczek, K. Macur, L. Bober, T. Frackowiak, A. Bucinski, D. Rystok-Grabska, J. Stasiak, K. Koba, Factor analysis of microbiological activity data and structural parameters of antibacterial quinolones, J. Mol. Model. 16 (2010) 327–335.
[2] M. Diaz, S. Calaforra, E. Ibanez, A. Giner, R. Almero, D. Sanz, A. Campos, Challenge tests with quinolones, Allergy 64 (2009) 291–292.
[3] K. Drlica, H. Hiasa, R. Kerns, M. Malik, A. Mustaev, X. Zhao, Quinolones: action and resistance updated, Curr. Top. Med. Chem. 9 (2009) 981–998.
[4] F. Santos, P. Abreu, H. Castro, I. Paixao, C. Cirne-Santos, V. Giongo, J. Barbosa, B. Simonetti, V. Garrido, D. Bou-Habib, D. Silva, P. Batalha, J. Temerozo, T. Souza, C. Nogueira, A. Cunha, C. Rodrigues, V. Ferreira, M. de Souza, Synthesis, antiviral activity and molecular modeling of oxoquinoline derivatives, Bioorg. Med. Chem. 17 (2009) 5476–5481.

[5] M. Dinakaran, P. Senthilkumar, P. Yogeeswari, A. China, V. Nagaraja, D. Sriram, Novel ofloxacin derivatives: synthesis, antimycobacterial and toxicological evaluation, Bioorg. Med. Chem. Lett. 18 (2008) 1229–1236.
[6] A. Boteva, O. Krasnykh, The methods of synthesis, modification, and biological activity of 4-quinolones (review), Chem. Heterocycl. Compd. 45 (2009) 757–785.
[7] Y. Kurasawa, K. Yoshida, N. Yamazaki, E. Kaji, K. Sasaki, Y. Hiwasa, A. Tsukamoto, H. Itoc, Quinolone analogues 10: synthesis of antimalarial quinolones having pyridyl moiety in N1-side chain, J. Heterocycl. Chem. 47 (2010) 657–663.
[8] H.J. Adam, N.M. Laing, C.R. King, B. Lulashnyk, D.J. Hoban, G.G. Zhanel, In vitro activity of nemonoxacin, a novel nonfluorinated quinolone, against 2,440 clinical isolates, Antimicrob. Agents Chemother. 53 (2009) 4915–4920.
[9] J. Azema, B. Guidetti, J. Dewelle, B. Le Calve, T. Mijatovic, A. Korolyov, J. Vaysse, M. Malet-Martino, R. Martino, R. Kiss, 7-((4-Substituted)piperazin-1-yl) derivatives of ciprofloxacin: synthesis and in vitro biological evaluation as potential antitumor agents, Bioorg. Med. Chem. 17 (2009) 5396–5407.
[10] A. Foroumadi, S. Emami, S. Rajabalian, M. Badinloo, N. Mohammadhosseini, A. Shafiee, N-Substituted piperazinyl quinolones as potential cytotoxic agents: structure-activity relationships study, Biomed. Pharmacother. 63 (2009) 216–220.
[11] M. Robinson, S. Elsea, B. Martin, T. Gootz, P. McGuirk, J. Sutcliffe, N. Osheroff, A novel quinolone with potent activity against eukaryotic DNA topoisomerase-II, Mol. Biol. DNA Topoisomer. Appl. Chemother. (1993) 189–198.
[12] M. Robinson, B. Martin, T. Gootz, P. McGuirk, M. Moynihan, J. Sutcliffe, N. Osheroff, Effects of quinolone derivatives on eukaryotic topoisomerase-II – a novel mechanism for enhancement of enzyme-mediated DNA cleavage, J. Biol. Chem. (1991) 14585–14592.
[13] Y. Chang, M. Hsu, S. Wang, L. Huang, K. Qian, S. Morris-Natschke, E. Hamel, S. Kuo, K. Lee, Design and synthesis of 2-(3-Benzo[*b*]thienyl)-6,7-methylenedioxyquinolin-4-one analogues as potent antitumor agents that inhibit tubulin assembly, J. Med. Chem. 52 (2009) 4883–4891.
[14] Y. Chang, J. Yang, S. Kuo, J. Chung, Induction of mitotic arrest and apoptosis by a novel synthetic quinolone analogue, CWC-8, via intrinsic and extrinsic apoptotic pathways in human osteogenic sarcoma U-2 OS cells, Anticancer Res. 29 (2009) 3139–3148.
[15] S. Jantová, A. Repický, Ľ. Čipák, 3-(5-Nitro-2-thienyl)-9-chloro-5-morpholin-4-yl[1,2,4]triazolo[4,3-*c*]quinazoline induces ROS-mitochondrial mediated death signaling and activation of p38 MAPK in murine L1210 leukemia cells, Neoplasma 56 (2009) 494–499.
[16] P.C. Sharma, A. Jain, S. Jain, Fluoroquinolone antibacterials: a review on chemistry, microbiology and therapeutic prospects, Acta Poloniae Pharm. 66 (2009) 587–604.
[17] P. Senthilkumar, M. Dinakaran, P. Yogeeswari, A. China, V. Nagaraja, D. Sriram, Antimycobacterial activities of novel fluoroquinolones, Biomed. Pharmacother. 63 (2009) 27–35.
[18] M. Andersson, A. MacGowan, Development of the quinolones, J. Antimicrob. Chemother. 51 (2003) 1–11.
[19] N. Hayashi, Y. Nakata, A. Yazaki, New findings on the structure-phototoxicity relationship and photostability of fluoroquinolones with various substituents at position 1, Antimicrob. Agents Chemother. 48 (2004) 799–803.
[20] N. Neumann, A. Blotz, G. Wasinska-Kempka, M. Rosenbruch, P. Lehmann, H. Ahr, H. Vohr, Evaluation of phototoxic and photoallergic potentials of 13 compounds by different in vitro and in vivo methods, J. Photochem. Photobiol. B: Biol. 79 (2005) 25–34.
[21] G. Sanchez, M. Hidalgo, J. Vivanco, J. Escobar, Induced and photoinduced DNA damage by quinolones: ciprofloxacin, ofloxacin and nalidixic acid determined by comet assay, Photochem. Photobiol. 81 (2005) 819–822.
[22] K. Yabe, K. Goto, T. Jindo, M. Sekiguchi, K. Furuhama, Structure-phototoxicity relationship in Balb/c mice treated with fluoroquinolone derivatives, followed by ultraviolet-A irradiation, Toxicol. Lett. 157 (2005) 203–210.
[23] J. Rosen, Proposed mechanism for the photodynamic generation of 8-oxo-7,8-dihydro-2′-deoxyguanosine produced in cultured cells by exposure to lomefloxacin, Mutat. Res. Fundam. Mol. Mech. Mutagen. 381 (1997) 117–129.
[24] J. Rosen, A. Prahalad, G. Schluter, D. Chen, G. Williams, Quinolone antibiotic photodynamic production of 8-oxo-7,8-dihydro-2′-deoxyguanosine in cultured liver epithelial cells, Photochem. Photobiol. 65 (1997) 990–996.
[25] B. Zhao, C.F. Chignell, M. Rammal, F. Smith, M.G. Hamilton, U.P. Andley, J.E. Roberts, Detection and prevention of ocular phototoxicity of ciprofloxacin and other fluoroquinolone antibiotics, Photochem. Photobiol. 86 (2010) 798–805.
[26] R. Stahlmann, Clinical toxicological aspects of fluoroquinolones, Toxicol. Lett. 127 (2002) 269–277.
[27] F. Vargas, T. Zoltan, A. Ramirez, T. Cordero, V. Chavez, C. Izzo, V. Lopez, Y. Cardenas, A. Fernandez, L. Hincapie, A. Fuentes, Studies of the photooxidant properties of antibacterial fluoroquinolones and their naphthalene derivatives, Pharmazie 64 (2009) 116–122.
[28] V. Lhiaubet-Vallet, F. Bosca, M. Miranda, Photosensitized DNA damage: the case of fluoroquinolones, Photochem. Photobiol. 85 (2009) 861–868.
[29] F. Lorenzo, S. Navaratnam, R. Edge, N.S. Allen, Primary photophysical properties of moxifloxacin – a fluoroquinolone antibiotic, Photochem. Photobiol. 84 (2008) 1118–1125.
[30] A. Albini, S. Monti, Photophysics and photochemistry of fluoroquinolones, Chem. Soc. Rev. 32 (2003) 238–250.
[31] L. Martinez, R. Sik, C. Chignell, Fluoroquinolone antimicrobials: singlet oxygen, superoxide and phototoxicity, Photochem. Photobiol. 67 (1998) 399–403.
[32] N. Umezawa, K. Arakane, A. Ryu, S. Mashiko, M. Hirobe, T. Nagano, Participation of reactive oxygen species in phototoxicity induced by quinolone antibacterial agents, Arch. Biochem. Biophys. 342 (1997) 275–281.
[33] P. Bilski, L. Martinez, E. Koker, C. Chignell, Influence of solvent polarity and proticity on the photochemical properties of norfloxacin, Photochem. Photobiol. 68 (1998) 20–24.
[34] L. Martinez, C. Chignell, Photocleavage of DNA by the fluoroquinolone antibacterials, J. Photochem. Photobiol. B: Biol. 45 (1998) 51–59.
[35] N. Agrawal, R. Ray, M. Farooq, A. Pant, R. Hans, Photosensitizing potential of ciprofloxacin at ambient level of UV radiation, Photochem. Photobiol. 83 (2007) 1226–1236.
[36] M. Wainwright, Photodynamic therapy: the development of new photosensitisers, Anticancer Agents Med. Chem. 8 (2008) 280–291.
[37] J.E. Brown, S.B. Brown, D.I. Vernon, Photosensitising drugs – their potential in oncology, Expert Opin. Investig. Drugs 8 (1999) 1967–1979.
[38] T. Dougherty, C. Gomer, B. Henderson, G. Jori, D. Kessel, M. Korbelik, J. Moan, Q. Peng, Photodynamic therapy, J. Nat. Cancer Inst. (1998) 889–905.
[39] Y. Tokura, Quinolone photoallergy: photosensitivity dermatitis induced by systemic administration of photohaptenic drugs, J. Dermatol. Sci. 18 (1998) 1–10.
[40] M. Heller, FDA alert of quinolones and phototoxicity, J. Drugs Dermatol. 7 (2008) 501.
[41] E. Fasani, A. Profumo, A. Albini, Structure and medium-dependent photodecomposition of fluoroquinolone antibiotics, Photochem. Photobiol. 68 (1998) 666–674.
[42] P. Černuchová, G. Vo-Thanh, V. Milata, A. Loupy, Solvent-free synthesis of quinolone derivatives, Heterocycles 64 (2004) 177–191.
[43] S. Jantová, S. Letašiová, V. Brezová, Ľ. Čipák, J. Lábaj, Photochemical and phototoxic activity of berberine on murine fibroblast NIH-3T3 and Ehrlich ascites carcinoma cells, J. Photochem. Photobiol. B: Biol. 85 (2006) 163–176.
[44] J. Rimarčík, V. Lukeš, E. Klein, A.M. Kelterer, V. Milata, Z. Vrecková, V. Brezová, Photoinduced processes of 3-substituted 6-fluoro-1,4-dihydro-4-oxoquinoline derivatives: a theoretical and spectroscopic study, J. Photochem. Photobiol. A: Chem. 211 (2010) 47–58.
[45] H. Kuhn, S. Braslavsky, R. Schmidt, Chemical actinometry, Pure Appl. Chem. (2004) 2105–2146.
[46] WinSIM, NIEHS, Research Triangle Park, NC USA 27709, 2002.
[47] J. Kováč, A. Krutošíková, R. Kada, Chemistry of Heterocyclic Compounds (in Slovak), Veda, Bratislava, 1982.
[48] G. Uščumlić, D. Mijin, N. Valentić, V. Vajs, B. Sušić, Substituent and solvent effects on the UV/Vis absorption spectra of 5-(4-substituted arylazo)-6-hydroxy-4-methyl-3-cyano-2-pyridones, Chem. Phys. Lett. (2004) 148–153.
[49] C. Hansch, A. Leo, R. Taft, A survey of hammett substituent constants and resonance and field parameters, Chem. Rev. 91 (1991) 165–195.
[50] J. Hirano, K. Hamase, K. Zaitsu, Evaluation of a simple and novel fluorescent anion sensor, 4-quinolone, and modification of the emission color by substitutions based on molecular orbital calculations, Tetrahedron 62 (2006) 10065–10071.
[51] F. Einschlag, L. Carlos, A. Capparelli, A. Braun, E. Oliveros, Degradation of nitroaromatic compounds by the UV-H_2O_2 process using polychromatic radiation sources, Photochem. Photobiol. Sci. 1 (2002) 520–525.
[52] F. Einschlag, J. Lopez, L. Carlos, A. Capparelli, A. Braun, E. Oliveros, Evaluation of the efficiency of photodegradation of nitroaromatics applying the UV/H_2O_2 technique, Environ. Sci. Technol. 36 (2002) 3936–3944.
[53] L. Zang, F. vanKuijk, B. Misra, H. Misra, The specificity and product of quenching singlet oxygen by 2,2,6,6-tetramethylpiperidine, Biochem. Mol. Biol. Int. 37 (1995) 283–293.
[54] A. De la Cruz, J. Elguero, P. Goya, A. Martinez, W. Pfleiderer, Tautomerism and acidity in 4-quinolone-3-carboxylic acid derivatives, Tetrahedron 48 (1992) 6135–6150.
[55] J. Rimarčík, K. Punyain, V. Lukeš, E. Klein, D. Dvoranová, A.-M. Kelterer, V. Milata, J. Lietava, V. Brezová, Theoretical and spectroscopic study of ethyl 1,4-dihydro-4-oxoquinoline-3-carboxylate and its 6-fluoro and 8-nitro derivatives in neutral and radical anion forms, J. Mol. Struct. 994 (2011) 61–69.
[56] C. Mitsos, A. Zografos, O. Igglessi-Markopoulou, Reactions of N-hydroxysuccinimide esters of anthranilic acids with anions of beta-keto esters. A new route to 4-oxo-3-quinolinecarboxylic acid derivatives, Chem. Pharm. Bull. 48 (2000) 211–214.
[57] D. Chu, A. Claiborne, J. Clement, J. Plattner, Syntheses and antibacterial activity of novel 6-fluoro-7-(gem-disubstituted piperazin-1-yl)-quinolines, Can. J. Chem. 70 (1992) 1328–1337.
[58] Y. Wang, K. Yu, S. Wang, Vibrational spectra study on quinolones antibiotics, Spectrochim. Acta A 65 (2006) 159–163.
[59] N. Abunada, H. Hassaneen, N. Kandile, O. Miqdad, Synthesis and antimicrobial activity of some new pyrazole, fused pyrazolo[3,4-d]-pyrimidine and pyrazolo[4,3-e][1,2,4]triazolo[1,5-*c*] pyrimidine derivatives, Molecules 13 (2008) 1501–1517.
[60] L. Pintilie, C. Negut, C. Oniscu, M. Caproiu, M. Nechifor, L. Iancu, C. Ghiciuc, R. Ursu, Synthesis and antibacterial activity of some novel quinolones, Romanian Biotechnol. Lett. 14 (2009) 4756–4767.
[61] J. Squella, L. Nunez-Vergara, R. Moscoso, J. Pezoa, J. Carbajo, Substituent effect of 4-nitroimidazole derivatives: acidic hydrogen as modulator of the nitro radical kinetic stability, J. Electrochem. Soc. 156 (2009) F60–F65.
[62] J. Arguello, L. Nunez-Vergara, S. Bollo, J. Squella, Nitro radical anion formation from nitrofuryl substituted 1,4-dihydropyridine derivatives in mixed and non-aqueous media, Bioelectrochemistry 69 (2006) 104–112.

[63] C. Yanez, J. Pezoa, M. Rodriguez, L. Nunez-Vergara, J. Squella, Voltammetric behavior of a 4-nitroimidazole derivative – nitro radical anion formation and stability, J. Electrochem. Soc. 152 (2005) J46–J51.
[64] P. Pieta, A. Petr, W. Kutner, L. Dunsch, In situ ESR spectroscopic evidence of the spin-trapped superoxide radical, $O_2^{\bullet -}$, electrochemically generated in DMSO at room temperature, Electrochim. Acta 53 (2008) 3412–3415.
[65] M. Rajendran, J. Inbaraj, R. Gandhidasan, R. Murugesan, Photodynamic action of damnacanthal and nordamnacanthal, J. Photochem. Photobiol. A: Chem. 162 (2004) 615–623.
[66] A. Rajendran, R. Gandhidasan, R. Murugesan, Photosensitisation and photoinduced DNA cleavage by four naturally occurring anthraquinones, J. Photochem. Photobiol. A: Chem. 168 (2004) 67–73.
[67] V. Brezová, S. Gabčová, D. Dvoranová, A. Staško, Reactive oxygen species produced upon photoexcitation of sunscreens containing titanium dioxide (an EPR study), J. Photochem. Photobiol. B: Biol. 79 (2005) 121–134.
[68] K. Stolze, N. Udilova, H. Nohl, Spin adducts of superoxide, alkoxyl, and lipid-derived radicals with EMPO and its derivatives, Biol. Chem. 383 (2002) 813–820.
[69] M. Zalibera, P. Rapta, A. Staško, L. Brindzová, V. Brezová, Thermal generation of stable $SO_4^{\bullet -}$ spin trap adducts with super-hyperfine structure in their EPR spectra: an alternative EPR spin trapping assay for radical scavenging capacity determination in dimethylsulphoxide, Free Radic. Res. 43 (2009) 457–469.
[70] G. Olive, A. Mercier, F. Le Moigne, A. Rockenbauer, P. Tordo, 2-Ethoxycarbonyl-2-methyl-3,4-dihydro-2H-pyrrole-1-oxide: evaluation of the spin trapping properties, Free Radic. Biol. Med. 28 (2000) 403–408.
[71] F. Chalier, P. Tordo, 5-Diisopropoxyphosphoryl-5-methyl-1-pyrroline N-oxide, DIPPMPO, a crystalline analog of the nitrone DEPMPO: synthesis and spin trapping properties, J. Chem. Soc. Perkin Trans. 2 (2002) 2110–2117.
[72] V. Brezová, M. Valko, M. Breza, H. Morris, J. Telser, D. Dvoranová, K. Kaiserová, Ľ. Varečka, M. Mazúr, D. Leibfritz, Role of radicals and singlet oxygen in photoactivated DNA cleavage by the anticancer drug camptothecin: an electron paramagnetic resonance study, J. Phys. Chem. B 107 (2003) 2415–2425.
[73] S. Goldstein, A. Samuni, Kinetics and mechanism of peroxyl radical reactions with nitroxides, J. Phys. Chem. A 111 (2007) 1066–1072.
[74] A. Samuni, S. Goldstein, A. Russo, J. Mitchell, M. Krishna, P. Neta, Kinetics and mechanism of hydroxyl radical and OH-adduct radical reactions with nitroxides and with their hydroxylamines, J. Am. Chem. Soc. 124 (2002) 8719–8724.
[75] J. Wadhawan, P. Welford, H. McPeak, C. Hahn, R. Compton, The simultaneous voltammetric determination and detection of oxygen and carbon dioxide – a study of the kinetics of the reaction between superoxide and carbon dioxide in non-aqueous media using membrane-free gold disc microelectrodes, Sens. Actuators B: Chem. 88 (2003) 40–52.
[76] T. Bevilaqua, T. Goncalves, C. Venturini, V. Machado, Solute-solvent and solvent-solvent interactions in the preferential solvation of 4-[4-(dimethylamino)styryl]-1-methylpyridinium iodide in 24 binary solvent mixtures, Spectrochim. Acta A 65 (2006) 535–542.
[77] T.A. Jenny, N.J. Turro, Solvent and deuterium isotope effects on the lifetime of singlet oxygen determined by direct emission spectroscopy at 1.27 μm, Tetrahedron Lett. 23 (1982) 2923–2926.
[78] S. Jantová, K. Koňariková, S. Letašiová, E. Paulovičová, V. Milata, V. Brezová, Photochemical and phototoxic properties of ethyl 1,4-dihydro-8-nitro-4-oxoquinoline-3-carboxylate, a new quinoline derivative, J. Photochem. Photobiol. B: Biol. 102 (2011) 77–91.
[79] J. Weaver, S. Porasuphatana, P. Tsai, T. Budzichowski, G.M. Rosen, Spin trapping nitric oxide from neuronal nitric oxide synthase: a look at several iron-dithiocarbamate complexes, Free Radic. Res. 39 (2005) 1027–1033.